DETECTION OF PULMONARY TUBERCULOSIS IN CHEST X-RAY USING DEEP LEARNING

Aqilah Rozhan[1], Anas Tharek[1]*, Izyan Ismail[2], Soo Tze Hui[1], Luthffi Idzhar Ismail[3], Atikah Farzanah Yamba[4], Sobri Muda[1], Noor Hayatul Al-Akmal Noralam[5]

[1] Department of Radiology, Faculty of Medicine and Health Sciences, Universiti Putra Malaysia (UPM)

[2] Department of Radiology, Hospital Serdang, Malaysia

[3] Department of Electrical & Electronic Engineering, Universiti Putra Malaysia (UPM)

[4] PadiMedical Sdn. Bhd., Serdang, Selangor, Malaysia

[5] Radiology Department, Hospital Sultan Abdul Aziz Shah (HSAAS), Faculty of Medicine and Health Sciences, Universiti Putra Malaysia (UPM), Serdang, Selangor, Malaysia

*Corresponding author: Anas Tharek

ABSTRACT

Pulmonary tuberculosis (PTB) remains a major global health concern, particularly in high-burden countries such as Malaysia. Chest X-ray (CXR) is the most accessible screening modality, but its interpretation is subjective and prone to inter-observer variability. This study aimed to develop and evaluate a deep learning–based algorithm using YOLOv8 for automated PTB detection on CXR and to assess the impact of data augmentation on diagnostic performance. A retrospective cross-sectional study of 1,000 anonymized CXR images from Hospital Serdang was conducted, with CXRs categorized into three classes: highly suspicious PTB, low suspicion PTB, and no active lung lesion. Data were divided into training (70%), testing (20%), and validation (10%) sets, and pre-processing included DICOM-to-JPEG conversion, anonymization, and augmentation techniques such as flipping, rotation, cropping, brightness, and grayscale adjustments. Model performance was evaluated using accuracy, precision, recall, F1-score, ROC and Precision–Recall (PR) curves, and Grad-CAM visualization for explainability. Without augmentation, YOLOv8 achieved 74% accuracy (precision 0.78, recall 0.74), while with augmentation, accuracy improved to 85%, recall for highly suspicious PTB increased from 0.75 to 0.87, and macro F1-score rose from 0.76 to 0.85.

ROC analysis demonstrated macro-average AUC improvement from 0.71 to 0.85, and PR curves showed micro-average AP rising from 0.55 to 0.74. Grad-CAM highlighted radiologically relevant areas such as upper-lobe consolidation and cavitary lesions, supporting clinical interpretability. Overall, the YOLOv8 model achieved diagnostic performance comparable to commercial CAD systems such as CAD4TB and Lunit INSIGHT, with data augmentation significantly enhancing sensitivity and generalization. This locally trained AI model demonstrates strong potential for scalable PTB screening, particularly in resource-limited settings.

Keywords: Artificial Intelligence; Deep Learning; YOLOv8; Pulmonary Tuberculosis; Chest X-Ray

1.0 INTRODUCTION

Tuberculosis (TB) remains one of the leading infectious diseases worldwide, caused by Mycobacterium tuberculosis (Mtb). Despite being curable and preventable, TB continues to represent a major global health burden, with an estimated 10.8 million new cases and 1.3 million deaths reported in 2023 [1]. Since 2021, TB incidence rates have increased after several years of decline, delaying progress toward the World Health Organization (WHO) End TB targets [1].

In Malaysia, TB remains an upper-moderate-burden disease. The incidence rate reached 113 cases per 100 000 population in 2022, the highest recorded in four decades, despite sustained national control efforts [2]. Although TB is treatable, delays in diagnosis and treatment initiation continue to hinder effective control of transmission and morbidity [2].

Chest X-ray (CXR) remains the most widely used imaging modality for the initial screening of pulmonary tuberculosis (PTB) due to its affordability, rapidity, and accessibility, especially in community-based and primary care settings. However, CXR interpretation is subjective and heavily dependent on radiologist expertise, with reported inter-observer variability ranging between 20% and 40% [3–5]. This variability, combined with a shortage of radiologists in resource-limited settings, contributes to inconsistent interpretations and delays in diagnosis [4].

Radiographic findings in PTB are heterogeneous and depend on the stage of the disease. Active

or reactivation TB frequently presents as upper-lobe consolidation, cavitation, or a "tree-in-bud" pattern, whereas healed or inactive TB often demonstrates fibrotic scarring, pleural thickening, or calcified granulomas [6]. These overlapping features make human interpretation difficult, especially when findings are subtle or confounded by other pulmonary pathologies.

Recent advances in artificial intelligence (AI) and deep learning (DL) have shown significant potential to improve diagnostic accuracy and consistency in radiological interpretation. Deep learning, particularly convolutional neural networks (CNNs), can automatically extract and learn hierarchical image features, allowing for reliable pattern recognition comparable to human-level expertise [5,7]. Several studies have demonstrated the ability of AI systems to detect TB with performance metrics equivalent to trained radiologists [8]. For example, Kazemzadeh et al. [8] reported that DL algorithms achieved high diagnostic accuracy in detecting PTB, while Nguyen et al. [9] introduced the VinDr-CXR dataset with over 18 000 annotated chest radiographs, which has become a benchmark for model training and validation in thoracic imaging research.

The WHO now recognizes AI-based computer-aided detection (CAD) systems as acceptable alternatives to human readers for CXR TB screening in areas where radiologists are scarce [10]. Commercial AI systems such as CAD4TB, Lunit INSIGHT CXR, and qXR have shown sensitivities of 55–70% and specificities of 83–90% [10,11], confirming their potential role in large-scale TB screening programs.

Among deep learning frameworks, the "You Only Look Once" (YOLO) family has become one of the most efficient for object detection and real-time image analysis. Unlike two-stage detectors such as R-CNN, YOLO performs object localization and classification simultaneously, offering high speed and accuracy [10]. The latest version, YOLOv8, introduced in 2023, integrates advanced architectural components, including CSPDarknet53 as the backbone, Path Aggregation Network (PANet) for feature fusion, and a decoupled head for refined predictions [12]. These improvements enable YOLOv8 to achieve superior precision and inference speed, making it suitable for radiological image interpretation.

To enhance model generalization and mitigate overfitting, data augmentation methods such as horizontal and vertical flipping, image rotation, cropping, brightness and contrast adjustment, and grayscale transformation are widely used [13]. These techniques simulate variations in

patient positioning and exposure settings commonly encountered in clinical imaging. Despite international advances, locally trained and validated AI models for TB detection remain limited in Malaysia. Differences in disease prevalence, imaging protocols, and population characteristics may influence algorithm performance. Thus, localized model development is necessary to ensure diagnostic reliability and clinical relevance.

This study aims to develop and evaluate a deep learning–based model using YOLOv8 to detect pulmonary tuberculosis on chest X-rays. The model classifies CXRs into three diagnostic categories—highly suspicious PTB, low suspicion PTB, and no active lung lesion—and assesses the influence of data augmentation on model performance. The ultimate objective is to create an accurate, scalable, and interpretable AI-assisted diagnostic tool that supports the WHO End TB Strategy [14].

2.0 MATERIALS AND METHODS

2.1 Study Design and Setting

This retrospective cross-sectional study was conducted at the Department of Radiology, Hospital Serdang, in collaboration with Hospital Pengajar Universiti Putra Malaysia (HPUPM) and the PadiMedical Innovative Medical Platform. A total of 1000 anonymized CXR images were collected from the Hospital Serdang Picture Archiving and Communication System (PACS). The images were categorized into three diagnostic classes: highly suspicious PTB, low suspicion PTB, and no active lung lesion. Data collection spanned from 2020 to 2023, and model development and validation were performed between February and September 2025.

2.2 Study Population

Eligible participants included adult patients aged 18 years and older who had undergone frontal chest radiography in either posteroanterior (PA) or anteroposterior (AP) projection. Cases with microbiologically confirmed PTB were labeled as positive, while normal CXRs served as controls. Patients below 18 years of age or those with images showing significant artefacts, motion blur, or over/under-exposure were excluded from the dataset.

2.3 Sample Size and Classification

The minimum sample size was estimated using the sensitivity and specificity method described by Bujang and Adnan [15], assuming a TB prevalence of 30% and target sensitivity and specificity of 90%. The required minimum number of images was 770; this study exceeded that number with 1000 CXRs, including approximately 231 PTB-positive and 769 non-PTB cases. Each radiograph was classified based on radiological findings: images showing upper-lobe consolidation, cavitation, or 'tree-in-bud' nodularity were labeled as highly suspicious PTB; those with fibrotic scarring or calcified granulomas were labeled as low suspicion PTB; and normal or unrelated findings were labeled as no active lung lesion.

2.4 Image Pre-processing and Dataset Preparation

All images were exported from PACS in DICOM format, anonymized to remove patient identifiers, and converted to JPEG format for model compatibility. Three radiologists independently reviewed and labeled each image, and only images with unanimous consensus were included. The dataset was randomly divided into training (70%), testing (20%), and validation (10%) subsets to ensure balanced model training and unbiased evaluation.

To improve model robustness, data augmentation was applied to the training dataset, including rotation up to ±15°, horizontal and vertical flipping, random cropping, brightness modification of ±20%, and grayscale conversion [13]. These transformations simulated realistic variations in patient positioning and exposure.

2.5 YOLOv8 Model Development

Model training was performed using the YOLOv8 framework, a single-stage detector that integrates feature extraction, fusion, and prediction in one network. The architecture includes CSPDarknet53 as the backbone for feature extraction, PANet as the neck for multi-scale fusion, and a detection head for object localization and classification [10,12]. Training was conducted using Jupyter Notebook with a Python-based deep learning environment. The model was trained on the augmented dataset with standardized hyperparameters, including batch size, learning rate, and epochs optimized for convergence. Training performance was monitored

using loss curves, accuracy metrics, and validation scores generated automatically at each epoch.

2.6 Explainable AI: Grad-CAM Visualization

To ensure interpretability of the model's decision-making process, Gradient-weighted Class Activation Mapping (Grad-CAM) was implemented. Grad-CAM generates heatmaps that highlight the regions within the CXR that most strongly influenced the model's prediction [16]. This technique helps clinicians verify that the algorithm's attention aligns with pathologically relevant lung regions, such as areas of consolidation or cavitation.

2.7 Model Evaluation

The trained model was evaluated using the confusion matrix to derive accuracy, precision, recall (sensitivity), and F1-score. These metrics were computed using the following formulas:

$$\text{Precision} = \frac{TP}{TP + FP}, \quad \text{Recall} = \frac{TP}{TP + FN}, \quad \text{F1} = \frac{2TP}{2TP + FP + FN}$$

Receiver Operating Characteristic (ROC) and Precision–Recall (PR) curves were plotted to assess the discrimination and predictive capability of the model. Because this study focused on overall image classification rather than lesion segmentation, localization metrics such as Intersection over Union (IoU) and mean Average Precision (mAP) were not utilized.

2.8 Ethical Considerations

Ethical approval was obtained from the National Medical Research Register (NMRR) and the Ethics Committee of Universiti Putra Malaysia. All images were anonymized prior to analysis to ensure data confidentiality and compliance with ethical standards for human research.

3.0 RESULTS AND DISCUSSION

A total of 1,000 chest radiographs were analyzed and divided into training, testing, and validation subsets in a 70:20:10 ratio, providing 700 images for training, 201 for testing, and 99 for validation. Each image was categorized into one of three diagnostic classes—highly

suspicious pulmonary tuberculosis (PTB), low suspicion PTB, or no active lung lesion—based on radiologist interpretation and microbiological confirmation. Standard pre-processing converted DICOM files into JPEG format, anonymized patient data, and normalized image dimensions. Data augmentation was subsequently applied to improve model generalization, using horizontal and vertical flipping, limited rotation (±15°), static cropping, brightness adjustment (–20 to +20 %), and partial grayscale transformation (Table 1). Representative augmented examples are shown in Figure 1.

Table 1. Augmentation techniques applied during training

Technique	Applied Parameters
Flip	Horizontal, Vertical
90° Rotate	Clockwise, Counter-Clockwise, Upside-down
Rotation	Between -15° and +15°
Grayscale	Apply to 24% of images
Brightness	Between -20% and +20%
Static Crop	24-82% horizontal region, 0-76% vertical region

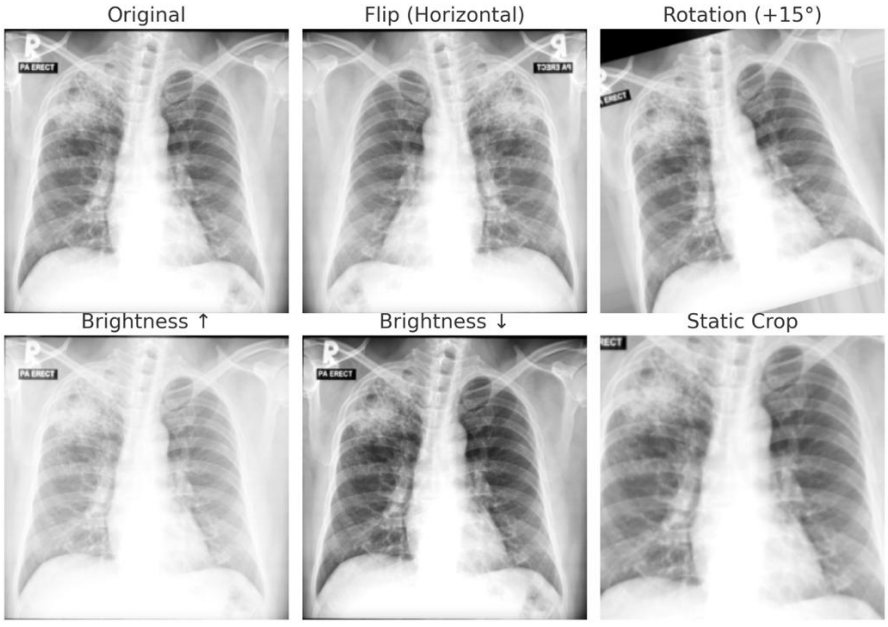

Figure 1. Examples of data augmentation applied to CXR, including flipping, rotation, brightness adjustment, and static cropping

3.1 Model Performance

The YOLOv8 classifier was evaluated under two conditions: training without augmentation and with augmentation. Without augmentation, the model achieved 74 % accuracy, correctly classifying 149 of 201 test cases (Figure 2A). Confusion matrix analysis revealed several misclassifications between highly suspicious and low-suspicion PTB categories, reflecting overlap in parenchymal findings such as fibrosis and residual opacities. With augmentation, the model correctly classified 170 of 201 cases, yielding an 85 % accuracy (Figure 2B). This improvement demonstrates the impact of augmented variability on the model's learning robustness.

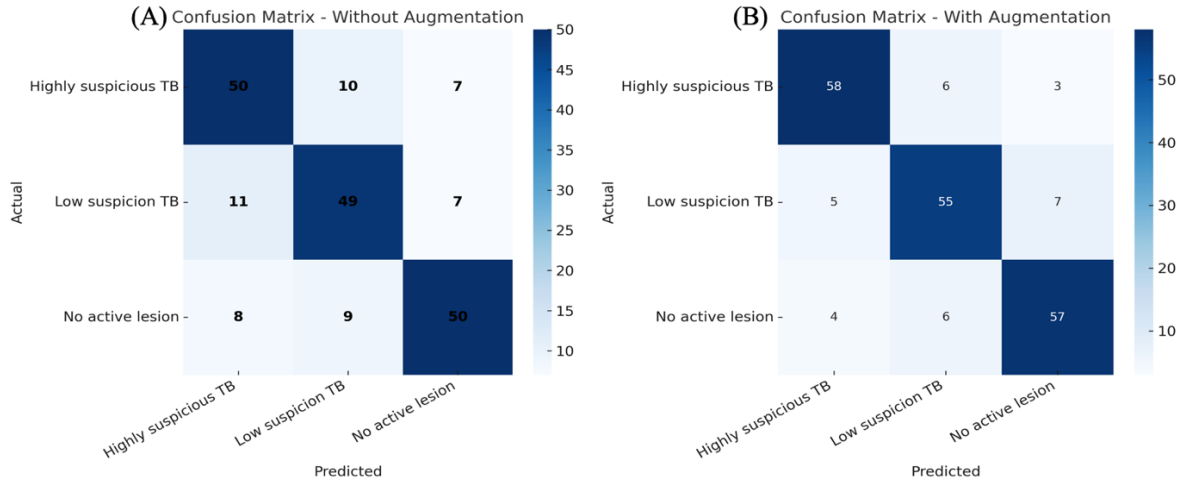

Figure 2. Confusion matrix of the YOLOv8 model trained without augmentation and with augmentation

Performance metrics are summarized in Table 2. Macro-precision, recall, and F1-score improved from 0.78, 0.74, and 0.76 to 0.84, 0.85, and 0.85, respectively. For highly suspicious PTB, recall increased from 0.75 to 0.87 and precision from 0.78 to 0.86, confirming that augmentation enhanced sensitivity while maintaining specificity. Similar gains were observed for low-suspicion PTB and no-active-lesion groups, indicating balanced generalization across classes.

Table 2. Comparison of class-wise performance metrics between non-augmented and augmented models

Metric	Without Augmentation	With Augmentation
Accuracy	74%	85%
Macro Precision	0.78	0.84
Macro Recall	0.74	0.85
Macro F1-score	0.76	0.85
Precision (Highly suspicious PTB)	0.78	0.86
Recall (Highly suspicious PTB)	0.75	0.87
F1-score (Highly suspicious PTB)	0.76	0.87
Precision (Low suspicion PTB)	0.77	0.82
Recall (Low suspicion PTB)	0.73	0.82
F1-score (Low suspicion PTB)	0.75	0.82
Precision (No active lung lesion)	0.78	0.85
Recall (No active lung lesion)	0.75	0.85
F1-score (No active lung lesion)	0.76	0.85

Receiver Operating Characteristic (ROC) analysis demonstrated improvement of the macro-average area under the curve (AUC) from 0.71 to 0.85 after augmentation (Figure 3). Precision–Recall (PR) curves showed an increase in micro-average average precision (AP) from 0.55 to 0.74 (Figure 4), suggesting fewer false negatives. Calibration curves (Figure 5) also aligned more closely with the ideal diagonal, indicating that augmented training improved probability reliability and clinical interpretability.

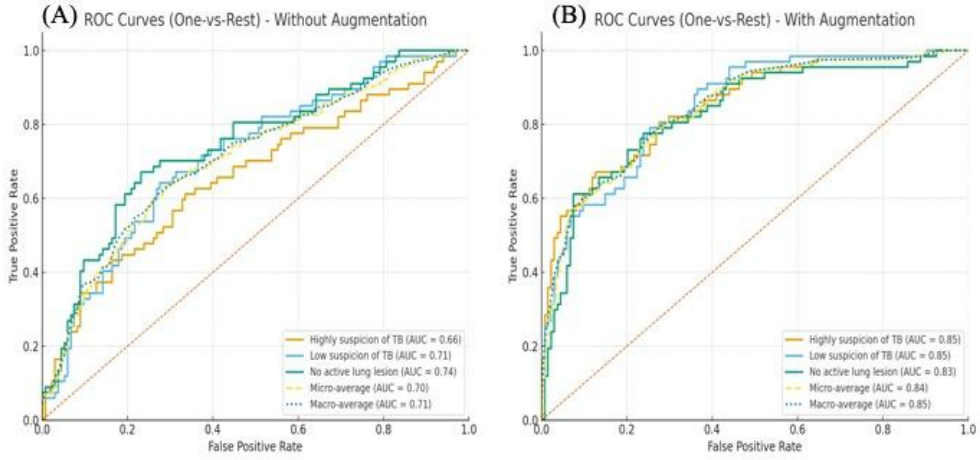

Figure 3. ROC curves of YOLOv8 model without augmentation and with augmentation

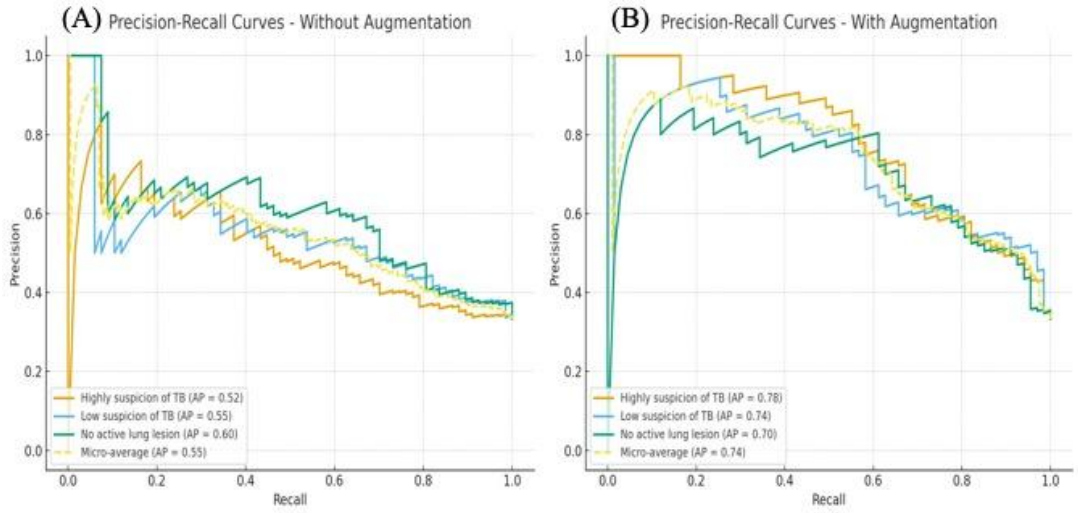

Figure 4. Precision–Recall curves of YOLOv8 model without augmentation and with augmentation

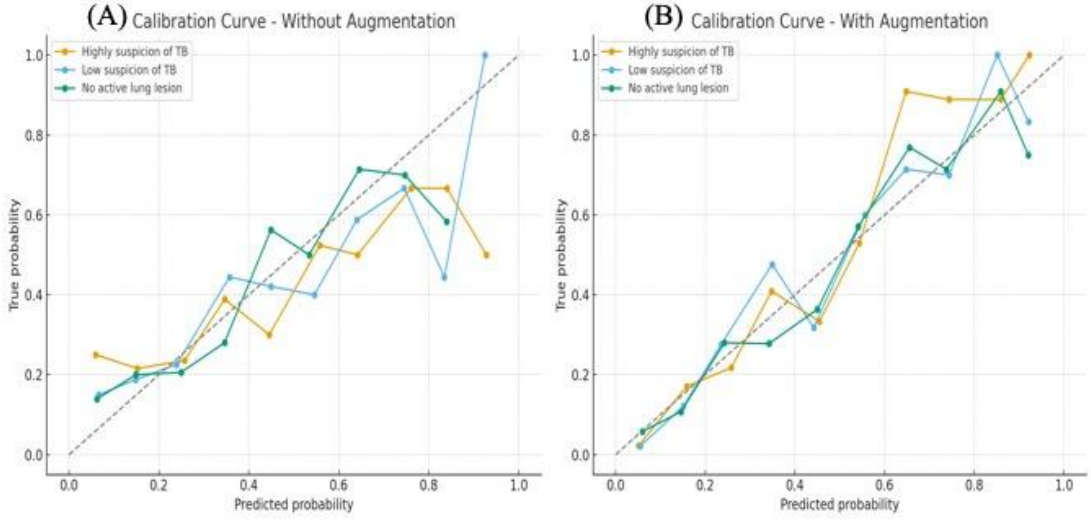

Figure 5. Calibration curves of YOLOv8 classification without augmentation and with augmentation

3.2 Model Explainability

To address the interpretability of deep learning predictions, Gradient-weighted Class Activation Mapping (Grad-CAM) was applied to visualize salient regions influencing model decisions (Figure 6). For radiographs classified as highly suspicious PTB, activation heatmaps exhibited strong red–yellow intensities over upper-lobe consolidations and cavitary lesions, validating that YOLOv8 focused on disease-relevant structures. Low-suspicion PTB cases

demonstrated moderate activations over fibrotic or perihilar regions, while normal CXRs exhibited minimal activation across lung fields. Misclassified examples revealed spurious activations over ribs or cardiac borders, underscoring areas where technical artifacts may confound detection. Overall, Grad-CAM enhanced transparency and clinician confidence by confirming physiologically plausible reasoning within the network.

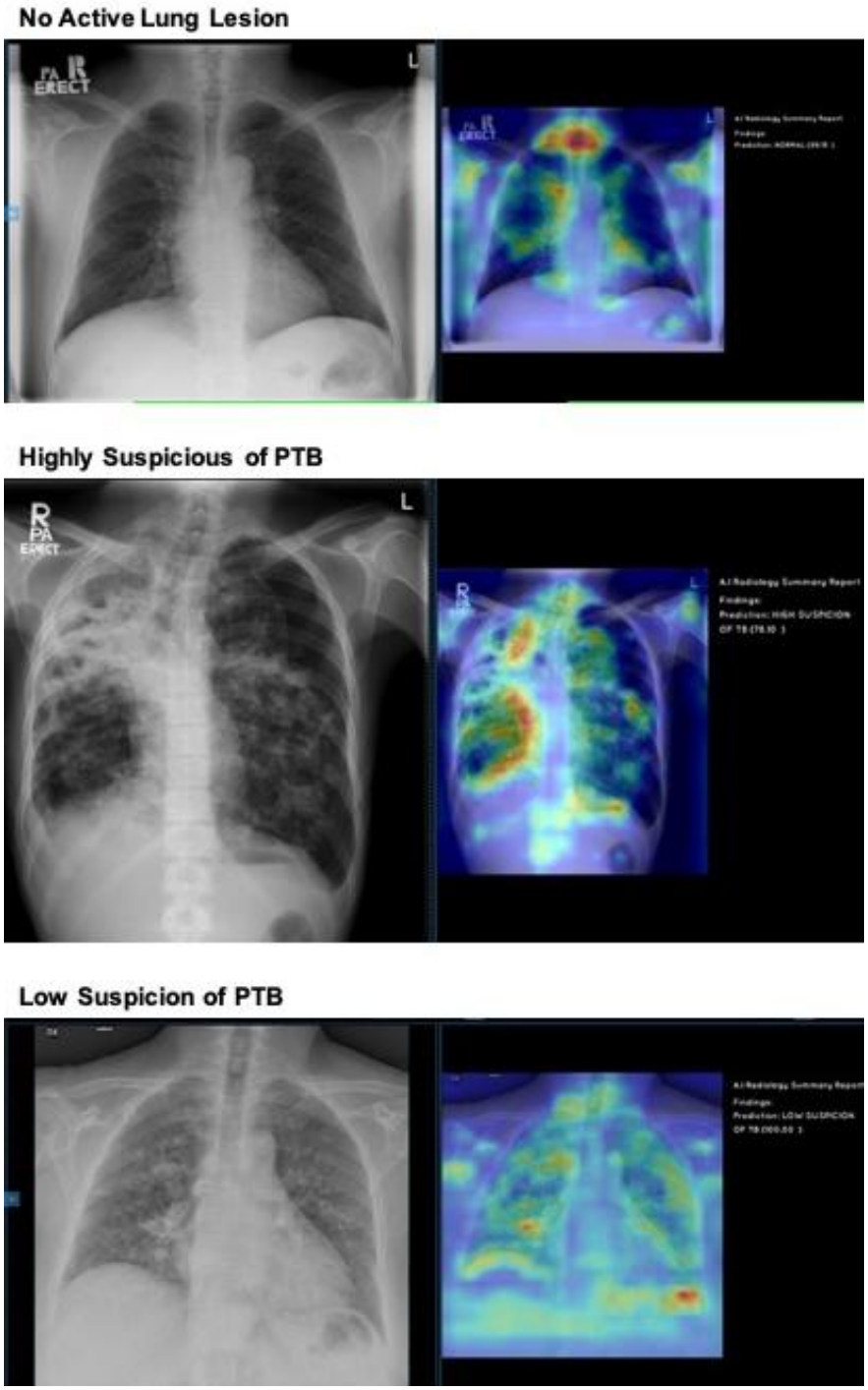

Figure 6. Grad-CAM visualization highlighting pulmonary lesions detected by the YOLOv8 model

3.3 Comparative Evaluation and Interpretation

The improved performance of YOLOv8 with augmentation compares favorably with existing computer-aided detection (CAD) systems. CAD4TB, evaluated in large-scale screening programs, has demonstrated sensitivities of 83–90 % and specificities of 55–70 % [17], while qXR and Lunit INSIGHT CXR report sensitivities above 89 % [18]. The augmented YOLOv8 model achieved a recall (sensitivity) of 0.87 and overall accuracy of 0.85—values within the diagnostic range of these WHO-endorsed systems. According to the World Health Organization Target Product Profile (TPP) for TB triage tests, ≥90 % sensitivity and ≥70 % specificity are acceptable thresholds [19]; the present model closely approaches this benchmark despite being trained on a smaller, locally sourced dataset.

Compared with similar academic efforts, these findings align with Kazemzadeh et al. (2023), who demonstrated radiologist-level deep-learning performance for PTB detection [8], and Nguyen et al. (2022), who emphasized the role of diverse annotated datasets [9]. The observed +11 % accuracy gain with augmentation corroborates prior studies that highlight dataset expansion as key to reducing overfitting [20, 21]. Augmentation therefore provides a cost-effective means to approximate the imaging variability otherwise obtainable only from multi-institutional datasets—an important advantage for low-resource environments.

3.4 Clinical and Public-Health Implications

From a clinical standpoint, improved recall is critical because undetected PTB cases drive continued transmission. An 87 % recall for highly suspicious PTB suggests that YOLOv8 could serve as an effective triage tool, flagging radiographs for expert review and thereby reducing radiologist workload in high-volume or resource-limited settings. Explainable heatmaps further increase trustworthiness, meeting WHO recommendations that AI tools be transparent, verifiable, and ethically deployable [16]. Integration into hospital PACS or mobile screening systems may enable large-scale, automated TB detection, complementing ongoing national End TB initiatives [1, 14].

3.5 Limitations and Future Work

Despite encouraging results, the study's single-center design and modest sample size (1,000 CXR) limit generalizability. Although augmentation mitigated data scarcity, multi-center validation is required to test robustness across different imaging protocols and populations. Moreover, this work focused on image-level classification rather than lesion localization. Future versions could incorporate bounding-box detection and multi-modal inputs combining CXR with clinical or laboratory data to enhance diagnostic precision.

4.0 CONCLUSION

This study demonstrated that a YOLOv8-based deep learning model can accurately detect pulmonary tuberculosis (PTB) on chest radiographs. Using a balanced dataset of 1,000 images, the model achieved 85% accuracy and 0.87 recall for highly suspicious PTB cases after data augmentation, compared with 74% accuracy and 0.75 recall without augmentation. These improvements confirm that data augmentation enhances model sensitivity and generalization. Receiver Operating Characteristic and Precision–Recall analyses showed better discrimination after augmentation, with the AUC rising from 0.71 to 0.85 and average precision from 0.55 to 0.74, comparable to established CAD systems such as CAD4TB, qXR, and Lunit INSIGHT. The integration of Grad-CAM provided visual explainability, highlighting disease-relevant regions and improving clinical interpretability.

Although limited by a single-center dataset and modest sample size, the results indicate that YOLOv8 can serve as a scalable and explainable AI tool for PTB screening. With larger multi-center validation and clinical deployment, this model could support early TB detection and contribute to national and global End TB initiatives.

Author Contributions

Conceptualization: Aqilah Binti Rozhan and Anas Tharek. Methodology: Aqilah Binti Rozhan, Izyan Ismail, and Soo Tze Hui. Model development: Luthffi Idzhar Ismail and Atikah Farzanah Yamba. Supervision: Anas Tharek. Writing—original draft preparation: Aqilah Binti Rozhan. Writing—review and editing: Anas Tharek. All authors have read and agreed to the published version of the manuscript.

Funding

This research received no external funding.

Ethical Approval

This study was approved by the National Medical Research Register (NMRR), Ministry of Health Malaysia.

Acknowledgments

The authors acknowledge Universiti Putra Malaysia, Hospital Serdang, and PadiMedical Sdn. Bhd. for technical and institutional support. Special thanks to the engineering and radiology teams for their collaboration.

Conflicts of Interest

The authors declare no conflict of interest.

REFERENCES

[1] World Health Organization. (2024). Global tuberculosis report 2024. Geneva: WHO. Available at: https://www.who.int/teams/global-programme-on-tuberculosis-and-lung-health/tb-reports/global-tuberculosis-report-2024

[2] Fadzil, F. A., Ramli, S. R., & Neoh, H. (2025). Tuberculosis in Malaysia: Disease timeline, epidemiology, control initiatives and outlook. Malaysian Journal of Pathology, 47(1): 1–16. Available at: http://www.mjpath.org.my/submit/uploads/siuwhlac99c0e4c7-Fariha-Adriana-binti-Fadzil.pdf

[3] Kaviani, P., Kalra, M.K., Digumarthy, S.R., Gupta, R.V., Dasegowda, G., Jagirdar, A., Gupta, S., Putha, P., Mahajan, V., Reddy, B., et al. (2022). Frequency of Missed Findings on Chest Radiographs (CXRs) in an International, Multicenter Study: Application of AI to Reduce Missed Findings. Diagnostics, 12:2382. https://doi.org/10.3390/diagnostics12102382

[4] Gefter, W.B., Post, B.A., Hatabu, H. (2023). Commonly Missed Findings on Chest Radiographs: Causes and Consequences. Chest, 163(3):650–661. https://doi.org/10.1016/j.chest.2022.10.039

[5] Skarakhodava, H., Krzewska, K., Floriańczyk, A., Romanowicz, E., Kołdyj, A., Ozdarska, A., Biernat, A., Lampart, M., Rupińska, A., Kozon, K. (2025). Artificial Intelligence in Chest X-Ray Diagnostics of Pneumonia: Opportunities to Reduce Medical Errors and Improve Clinical Practice Efficiency. International Journal of Innovative Technologies in Social Science, 1. https://doi.org/10.31435/ijitss.3(47).2025.3500

[6] Al Ubaidi, B.A. (2018). The Radiological Diagnosis of Pulmonary Tuberculosis (TB) in Primary Care. Journal of Family Medicine and Disease Prevention, 4:073. https://doi.org/10.23937/2469-5793/1510073

[7] Malaysian Ministry of Health. (2022). Health Technology Assessment Report: Computer-aided detection/artificial intelligence for chest X-ray in early detection of tuberculosis. Putrajaya: Medical Development Division, MOH.

[8] Kazemzadeh, S., Yu, J., Jamshy, S., Pilgrim, R., Nabulsi, Z., Chen, C., Beladia, N., Lau, C., McKinney, S. M., Hughes, T., Kiraly, A. P., Kalidindi, S. R., Muyoyeta, M., Malemela, J., Shih, T., Corrado, G. S., Peng, L., Chou, K., Chen, P.-H. C., Liu, Y., Eswaran, K., Tse, D., Shetty, S., and Prabhakara, S., Deep learning detection of active pulmonary tuberculosis at chest radiography matched the clinical performance of radiologists, Radiology, 306(1), 2023, pp. 124–137.

[9] Nguyen, H. Q., Lam, K., Le, L. T., et al., VinDr-CXR: An open dataset of chest X-rays with radiologist's annotations, Scientific Data, 9, 2022, p. 429, https://doi.org/10.1038/s41597-022-01498-w

[10] Ali, M. L., and Zhang, Z., The YOLO framework: A comprehensive review of evolution, applications, and benchmarks in object detection, Computers, 13(12), 2024, p. 336, https://doi.org/10.3390/computers13120336

[11] Geric, C., Qin, Z. Z., Denkinger, C. M., Kik, S. V., Marais, B., Anjos, A., David, P. M., Ahmad Khan, F., and Trajman, A., The rise of artificial intelligence reading of chest X-rays for enhanced TB diagnosis and elimination, International Journal of Tuberculosis and Lung Disease, 27(5), 2023, pp. 367–372, https://doi.org/10.5588/ijtld.22.0687

[12] Ju, R.-Y. and Cai, W., Fracture detection in pediatric wrist trauma X-ray images using YOLOv8 algorithm, Scientific Reports, 13, 2023, p. 20077, https://doi.org/10.1038/s41598-023-47460-7

[13] Shorten, C., Khoshgoftaar, T.M. A survey on Image Data Augmentation for Deep Learning. J Big Data 6, 60 (2019). https://doi.org/10.1186/s40537-019-0197-0

[14] Ministry of Health Malaysia. (2023). Health White Paper (Kertas Putih Kesihatan). Putrajaya: Ministry of Health Malaysia. Available at: https://www.moh.gov.my/moh/resources/Penerbitan/Penerbitan%20Utama/Kertas%20Putih%20Kesihatan/Kertas_Putih_Kesihatan_(ENG)_compressed.pdf

[15] Bi, J., Li, K., Zheng, X., Zhang, G., and Lei, T., SPDC-YOLO: An efficient small target detection network based on improved YOLOv8 for drone aerial image, Remote Sensing, 17,

2025, p. 685, https://doi.org/10.3390/rs1719040685 [20] Shad, I., Zhang, Z., Asim, M., Al-Habib, M., Chelloug, S. A., and Abd El-Latif, A., Deep learning-based image processing framework for efficient surface litter detection in computer vision applications, Journal of Radiation Research and Applied Sciences, 18(2), 2025, 101534, ISSN 1687-8507, https://doi.org/10.1016/j.jrras.2025.101534

[16] Talaat, F. M., Gamel, S. A., El-Balka, R. M., Shehata, M., and ZainEldin, H., Grad-CAM enabled breast cancer classification with a 3D Inception-ResNet V2: Empowering radiologists with explainable insights, Cancers (Basel), 16(21), 2024, p. 3668, https://doi.org/10.3390/cancers16213668

[17] Nzimande, N., Murphy, K., Reither, K., Bosman, S., Ayakaka, I., Glass, T. R., Vanobberghen, F., Jacobs, B. K. M., Signorell, A., & Ncayiyana, J. (2025). Performance of CAD4TB artificial intelligence technology in TB screening programmes among the adult population in South Africa and Lesotho. Journal of Clinical Tuberculosis and Other Mycobacterial Diseases, 40: 100540. https://doi.org/10.1016/j.jctube.2025.100540

[18] Qin, Z. Z., Ahmed, S., Sarker, M. S., Paul, K., Adel, A. S. S., Naheyan, T., Barrett, R., Banu, S., & Creswell, J. (2021). Tuberculosis detection from chest X-rays for triaging in a high tuberculosis-burden setting: An evaluation of five artificial intelligence algorithms. The Lancet Digital Health, 3(9): e543–e554. https://doi.org/10.1016/S2589-7500(21)00116-3

[19] World Health Organization. (2023). Target product profiles for tests for tuberculosis treatment monitoring and optimization. Geneva: World Health Organization. Licence: CC BY-NC-SA 3.0 IGO.

[20] W. Almattar and A. Algherairy, "Investigating Image Augmentation for Classification of Chest X-Ray Images," 2022 14th International Conference on Computational Intelligence and Communication Networks (CICN), Al-Khobar, Saudi Arabia, 2022, pp. 65-71, doi: 10.1109/CICN56167.2022.10008268.

[21] Moles, L., Andres, A., Echegaray, G., & Boto, F. (2024). Exploring Data Augmentation and Active Learning Benefits in Imbalanced Datasets. Mathematics, 12(12), 1898. https://doi.org/10.3390/math12121898